

Automatic Yield-Line Analysis of Practical Slab Configurations via Discontinuity Layout Optimization

Linwei He¹; Matthew Gilbert, M.ASCE²; and Marcus Shepherd³

Abstract: The yield-line method provides a powerful means of rapidly estimating the ultimate load that can be carried by a reinforced concrete slab. The method can reveal hidden reserves of strength in existing slabs and can lead to highly economic slabs when used in design. Originally conceived before the widespread availability of computers, the yield-line method subsequently proved difficult to computerize, limiting its appeal in recent years. However, it was recently demonstrated that the discontinuity layout optimization (DLO) procedure could be used to systematically automate the method, and various isotropically reinforced, uniformly loaded slab examples were used to demonstrate this. The main purpose of this paper is to demonstrate that the DLO procedure can also be applied to a wide range of more practical slab problems, for example involving orthotropic reinforcement, internal columns, and point, line, and patch loads. The efficacy of the procedure is demonstrated via application to a variety of example problems from the literature; for all problems considered solutions are presented that improve upon existing numerical solutions. Furthermore, in a number of cases, solutions derived using previously proposed automated yield-line analysis procedures are shown to be highly nonconservative. DOI: 10.1061/(ASCE)ST.1943-541X.0001700. This work is made available under the terms of the Creative Commons Attribution 4.0 International license, <http://creativecommons.org/licenses/by/4.0/>.

Author keywords: Yield-line analysis; Plastic analysis; Discontinuity layout optimization; Slabs; Rationalization; Analysis and computation.

Introduction

The yield-line method of analysis (Johansen 1943) is a long-established and extremely powerful tool for estimating the maximum load sustainable by a reinforced concrete slab. To apply the method successfully, traditionally users have had to know something about the rules governing the construction of viable yield-line patterns, though these rules can be memorized, and for simple problems a hand analysis is quick and easy to perform. The guidance document produced by the U.K. Concrete Centre (Kennedy and Goodchild 2004) discusses the many benefits of yield-line design, in particular highlighting the highly economic reinforcement layouts that can result from its application (though it should be noted that the method considers flexural failure only, and serviceability considerations, which will sometimes govern the design, are not considered). Furthermore, various other guidance documents are available to assist new users, some of which also include useful formulas covering standard cases.

However, in many practical cases it can be difficult to identify the critical yield-line pattern by hand. This is true when the slab under consideration has an unusual geometry, reinforcement configuration, or pattern of applied loading. The presence of fixed (or so-called clamped) edges can also cause difficulties since in reality

complex yield-line patterns (e.g., involving corner fans) will often be critical in such cases, and these can be difficult to deal with in a hand analysis. Most importantly, it must be borne in mind that the yield-line method is an upper-bound method in the context of the fundamental theorems of plasticity, which means that an incorrectly chosen yield-line pattern will result in an unsafe estimate of the strength of the slab under consideration.

To address this issue, an automated method of identifying critical yield-line patterns was first proposed in the 1970s by Chan (1972), then working at the University of Oxford, and subsequently by Munro and Da Fonseca (1978), working at Imperial College, London. Both groups of researchers discretized the slab under consideration into rigid elements separated by potential yield-lines and then used linear programming (LP) techniques to identify the critical yield-line pattern. Unfortunately, when using rigid elements it can be observed that the solutions obtained depend on the layout of the mesh discretization employed. This means that in many cases progressively reducing the size of the mesh does not lead to convergence toward the exact solution [e.g., as demonstrated in the recent study by Bleyer and De Buhan (2013)]. Various groups of researchers, for example, Johnson and coworkers (Johnson 1994; Ramsay and Johnson 1998) and Thavalingam et al. (1999), attempted to address this through the use of a two-stage procedure. This involved supplementing the original rigid element procedure with a geometry-optimization phase, allowing the positions of nodes to be adjusted to try to improve the solution. The main drawback is that such procedures rely on the initial solution being of the same form as the true optimal layout. This is not necessarily the case, and, in mathematical optimization terms, such procedures will therefore be prone to identifying solutions that are locally rather than globally optimal [e.g., Johnson (1994) conceded that his proposed two-stage approach “does not directly generate likely critical collapse modes”].

In the absence of general tools, various automated hand calculation yield-line analysis methods have been developed, such as the COncrete BRidge ASsessment (Cobras) package developed by Middleton (1997) specifically for bridge assessment. This proved to be a very useful tool, showing that many existing reinforced

¹Research Associate, Dept. of Civil and Structural Engineering, Univ. of Sheffield, Sir Frederick Mappin Bldg., Mappin St., Sheffield S1 3JD, U.K. E-mail: linwei.he@sheffield.ac.uk

²Professor, Dept. of Civil and Structural Engineering, Univ. of Sheffield, Sir Frederick Mappin Bldg., Mappin St., Sheffield S1 3JD, U.K. (corresponding author). ORCID: <http://orcid.org/0000-0003-4633-2839>. E-mail: m.gilbert@sheffield.ac.uk

³Engineer, Arup, Rose Wharf, 78 East St., Leeds LS9 8EE, U.K. E-mail: Marcus.Shepherd@arup.com

Note. This manuscript was submitted on August 20, 2015; approved on September 19, 2016; published online on March 1, 2017. Discussion period open until August 1, 2017; separate discussions must be submitted for individual papers. This paper is part of the *Journal of Structural Engineering*, © ASCE, ISSN 0733-9445.

concrete slab bridges possessed significantly greater capacity than indicated by elastic analysis methods. However, because the tool relies on the use of an in-built library of predefined yield-line patterns, it is only suitable for analyzing a restricted range of slab geometries.

In parallel, various methods that seek to identify lower bound solutions have been investigated, such as those presented by Anderheggen and Knöpfel (1972), Krabbenhoft and Damkilde (2003), and, more recently, by Le et al. (2010) and Maunder and Ramsay (2012). However, it should be noted that these methods are comparatively complex since they involve the use of a nonlinear yield function and in addition are incapable of identifying discrete yield-lines directly [though these can be manually inferred from the output, as undertaken in the two-step slab analysis procedure recently described by Jackson and Middleton (2013)].

Given the inherent limitations of existing techniques, the opportunity was recently taken to apply the discontinuity layout optimization (DLO) procedure (Smith and Gilbert 2007) to the analysis of reinforced concrete slabs. Although full details are provided by Gilbert et al. (2014), in the present paper key features of the procedure are briefly outlined. It is then demonstrated that the procedure may straightforwardly be extended to treat practical slab analysis problems, involving orthotropic reinforcement, a wider variety of support conditions, and slabs that are subject to point, line, and patch loads. Additionally, it is shown that a recently developed rationalization procedure (He and Gilbert 2016) can be used to enhance the solutions obtained. In this paper the DLO-based procedure is applied to both benchmark problems from the literature and to more practical slab configurations, the aim being to clearly demonstrate its accuracy and usefulness.

Discontinuity Layout Optimization Formulation

A complete DLO analysis comprises several steps (Fig. 1). First, the slab is discretized using nodes spatially distributed across the problem domain [Fig. 1(b)], which are then interconnected with potential yield-lines [Fig. 1(c)]. Each yield-line employs the variables shown in Fig. 2: normal rotation θ_n along yield-line, twisting rotation θ_t , and out-of-plane displacement δ . With respect to these displacement variables, a linear programming (LP) problem comprising an objective function and constraints can be formulated as follows (after Gilbert et al. 2014):

$$\text{Minimize } \lambda \mathbf{f}_L^T \mathbf{d} = -\mathbf{f}_D^T \mathbf{d} + \mathbf{g}^T \mathbf{p} \quad (1a)$$

$$\text{Subject to } \mathbf{B} \mathbf{d} = \mathbf{0} \quad (1b)$$

$$\mathbf{N} \mathbf{p} - \mathbf{d} = \mathbf{0} \quad (1c)$$

$$\mathbf{f}_L^T \mathbf{d} = 1 \quad (1d)$$

$$\mathbf{p} \geq \mathbf{0} \quad (1e)$$

where \mathbf{d} and \mathbf{p} = vectors containing respectively the aforementioned displacement variables and corresponding nonnegative plastic multiplier variables. In the objective function of Eq. (1a), λ is a dimensionless load factor, here applied only to live loads; $\lambda \mathbf{f}_L^T \mathbf{d}$ and $\mathbf{f}_D^T \mathbf{d}$ describe the external work done, respectively, by live and dead loads (calculated in DLO by considering the effects

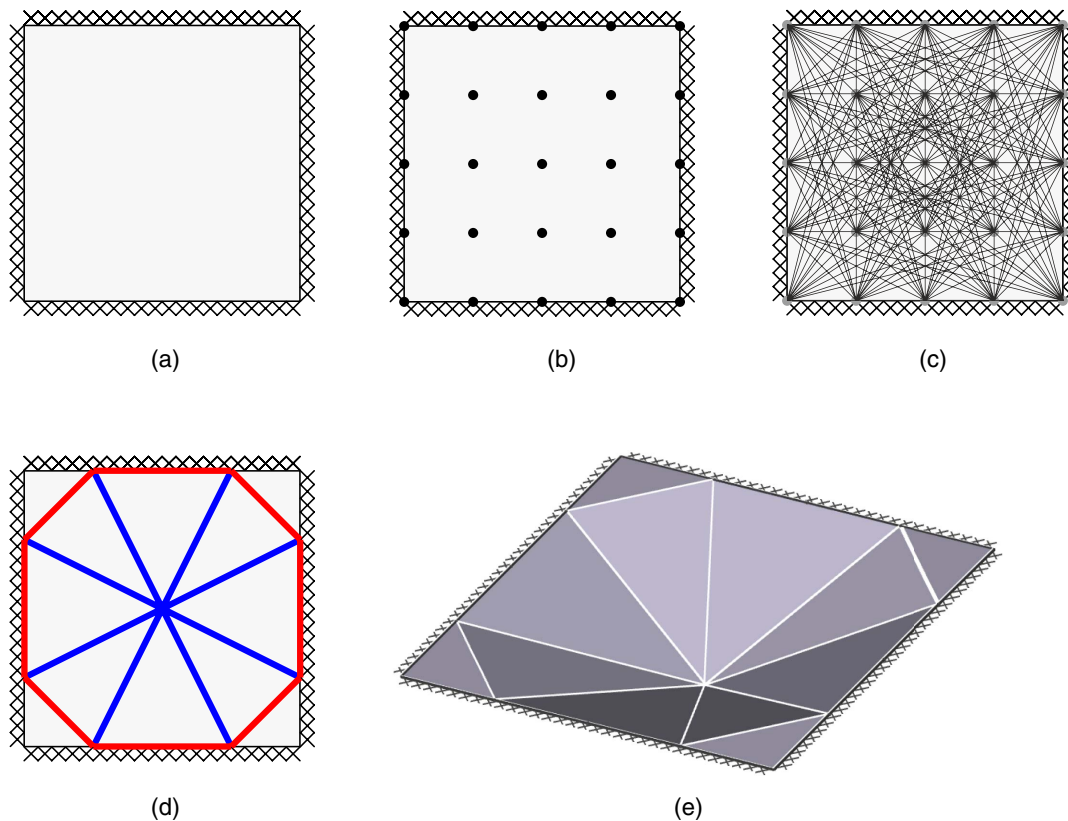


Fig. 1. Steps in DLO process: a simple example (reprinted from Gilbert et al. 2015, with permission): (a) Step 1: the geometry, boundary conditions, loads, and yielding moments are defined; (b) Step 2: nodal discretization (using four nodal divisions); (c) Step 3: nodes are connected by potential yield-lines; (d) Step 4: identify the subset of yield-lines present in the critical collapse mechanism using linear programming (LP); (e) Step 5 (optional): visualize deformed shape

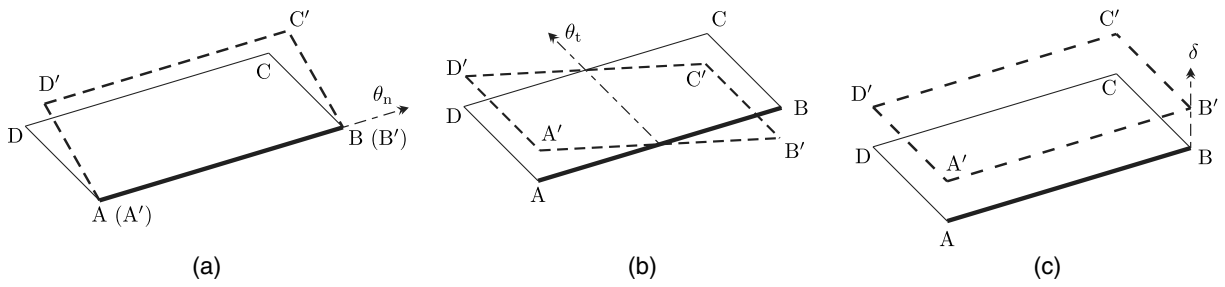
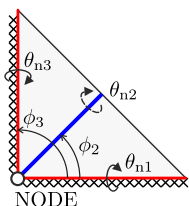


Fig. 2. Displacement variables for a yield-line AB (assuming block ABCD moves to A'B'C'D'): (a) normal rotation along yield-line; (b) twisting rotation; (c) out-of-plane displacement

Load type	Pressure	Point load	Line load	Patch load
Rotational moment f_{ni}	qAd_n	Pd_n	$w d_l d_n$	Qd_n
Torsional moment f_{ti}	qAd_t	Pd_t	$w d_l d_t$	Qd_t
Shear force f_i	qA	P	$w d_l$	Q

Fig. 3. Evaluating effects of loads lying in a strip “above” yield-line i

of loads lying in strips “above” each yield-line; the coefficients in \mathbf{f}_L and \mathbf{f}_D for the load types considered in this paper are provided in Fig. 3). Also, $\mathbf{g}^T \mathbf{p}$ describes the internal energy dissipation along yield-lines. In Eq. (1b), \mathbf{B} is a compatibility matrix used to ensure that yield-line displacements are kinematically admissible; see also Fig. 4. In Eq. (1c), \mathbf{N} is a plastic flow rule matrix describing the relation between the yield-line displacements in \mathbf{d} and their associated plastic multipliers \mathbf{p} . Also, in Eq. (1d), the external work done by a live load is normalized to ensure that λ directly defines the load factor. By solving the linear optimization problem given by Eqs. (1a)–(1e), the load factor at collapse and the associated yield-line pattern can be obtained. The deformed shape can also be plotted [Fig. 1(e)] to clearly indicate the form of the predicted failure mechanism.



$$\sum_{i=1}^3 \theta_{ni} \cos \phi_i = 0$$

$$\sum_{i=1}^3 \theta_{ni} \sin \phi_i = 0$$

Fig. 4. Compatibility requirements for yield-lines meeting at a node

Whereas the example shown in Fig. 1 contains very few nodes, in practice much denser nodal grids can be employed to obtain more accurate solutions. However, a side effect of this is that the resulting yield-line patterns can become quite complex in form. To simplify these, a postprocessing rationalization step, which involves adjusting the positions of the nodes via geometry optimization, can optionally be performed (He and Gilbert 2016). Unlike previously proposed methods that require a manual interpretation step (e.g., Johnson 1995; Jackson and Middleton 2013), here the rationalization is performed automatically following completion of a standard DLO analysis, generating yield-line patterns that are both simplified (i.e., contain fewer nodes and yield-lines) and more critical (i.e., the solutions are better). The extensions to the mathematical derivations described in He and Gilbert (2016) required to enable treatment of the practical slabs considered in the present paper are provided in Appendix I.

Modeling Features of Practical Slabs

Orthotropic Slab Reinforcement

In engineering practice, many slabs contain orthotropic reinforcement; such slabs were not considered in Gilbert et al. (2014). However, it will be shown here that orthotropic reinforcement can be

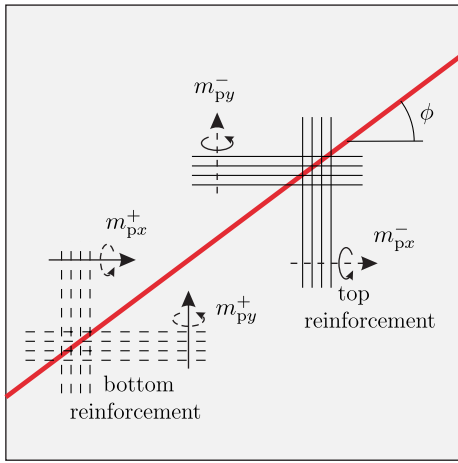


Fig. 5. Yield moments m_{px}^+ , m_{py}^+ , m_{px}^- , and m_{py}^- in an orthotropically reinforced concrete slab

handled using the DLO method. Referring to Fig. 5, suppose m_{px}^+ , m_{py}^+ and m_{px}^- , m_{py}^- are, respectively, the x - and y -direction positive and negative plastic moments of resistance per unit length. Also, m_p^+ and m_p^- are the plastic moments of resistance per unit length along a yield-line inclined at an angle of ϕ to the x -axis. Using the stepped yield-criterion approach proposed by Johansen (1943), the latter can be calculated from

$$m_p^+ = m_{px}^+ \cos^2 \phi + m_{py}^+ \sin^2 \phi \quad (2)$$

$$m_p^- = m_{px}^- \cos^2 \phi + m_{py}^- \sin^2 \phi \quad (3)$$

In the DLO formulation (Gilbert et al. 2014), the preceding equations can be used when calculating the internal energy dissipation terms for a given yield-line [i.e., the coefficients in \mathbf{g} , used in the objective function given by Eq. (1a)]. Note that since the orientation of a given yield-line connecting two nodes is known in advance, computing the energy dissipation terms is straightforward; hence, orthotropically reinforced slabs can be treated without difficulty in DLO.

Boundary Conditions

In Gilbert et al. (2014) and He and Gilbert (2016), only four boundary conditions were considered [free, symmetry, fixed, and simple

(anchored) boundaries; see the first four columns in Fig. 6]. However, in engineering practice, other boundary conditions are frequently encountered; the remaining columns in Figs. 6 and 7 provide details of the additional boundary conditions considered here. Additionally, here an optional support strength factor i is applied in the case of fixed supports [i is then a multiplier in internal energy dissipation terms in the objective function given by Eq. (1a)]. Further explanation of the remaining boundary conditions follows:

1. Nonanchored simple supports

An external simple support can be anchored or nonanchored; in the latter case, uplift may occur, which means that twisting and out-of-plane displacements can now be nonzero, with $\theta_t l / 2 \pm \delta \geq 0$ ensuring that uplift (only) can occur.

2. Knife-edge supports

These types of support may be located internally beneath the slab, with the slab above the support being *continuous*. This means that the slab can rotate along the support. If there exists no *relative* normal rotation at the support (i.e., $\theta_n = 0$), then no yield-line is allowed to form at the support. If $\theta_n \neq 0$, then a yield-line may develop along the support and internal energy dissipation needs to be accounted for. Regarding the twisting rotation θ_t and out-of-plane displacement δ , both (a) anchored and (b) nonanchored knife-edge supports are considered here. In the latter case, twisting and out-of-plane displacements can now be nonzero, and uplift can be allowed to occur (as with the nonanchored simple supports).

3. Column supports

Columns are frequently used in engineering practice; these can effectively be modeled using a combination of the aforementioned line support types. An external column is normally modeled using a simple support, while internal columns can now be modeled using either enclosed knife-edge supports or, if an internal column passes through the slab, by fixed supports (since the slab region is now discontinuous). In the latter case an optional support strength factor i can be applied. A summary of all column support types is shown in Fig. 7.

Application of Automated Method

Steps in the DLO procedure are shown in Fig. 1; a *MATLAB* script implementing the basic procedure is provided as supplemental data for interested readers. Dense nodal grids can be employed using a modern desktop computer, so that highly accurate numerical solutions can, if necessary, be obtained. To solve standard DLO

Support type	Free	Symmetry	Fixed ^a	Simple (anchored)	Simple (non-anchored)	Knife-edge (anchored)	Knife-edge (nonanchored)
Symbol	—————	— · — · — ·	XXXXXXXX	///////	\\ \\ \\ \\ \\	///////	\\ \\ \\ \\ \\
Displacement constraints (θ_t and δ)	None	None	$\theta_t = \delta = 0$	$\theta_t = \delta = 0$	$\frac{\theta_t l}{2} \pm \delta \geq 0$	$\theta_t = \delta = 0$	$\frac{\theta_t l}{2} \pm \delta \geq 0$
Type of normal rotation θ_n	Relative to support	Relative to support	Relative to support	Relative to support	Relative to support	Relative to interior of slab	Relative to interior of slab
Internal energy dissipation	0	$m_p \theta_n l$	$i m_p \theta_n l$	0	0	$m_p \theta_n l$	$m_p \theta_n l$

^a Variable support strength = $i m_p$

Fig. 6. Summary of line support types

Column type	External		Internal	
		Type I (supporting and anchoring slab)	Type II (supporting but not anchoring slab)	Type III (passing through slab)
Symbol	•			
Description	Formed by a short simple support	Formed by enclosed anchored knife-edge supports; slab is continuous	Formed by enclosed nonanchored knife-edge supports; slab is continuous	Formed by enclosed fixed supports ^[a] ; slab is discontinuous at column
Displacement constraints along edges	$\theta_t = \delta = 0$	$\theta_t = \delta = 0$	$\frac{\theta_t l}{2} \pm \delta \geq 0$	$\theta_t = \delta = 0$
Internal energy dissipation along edges	0	$m_p \theta_n l$	$m_p \theta_n l$	$im_p \theta_n l$

^a Variable support strength = im_p

Fig. 7. Summary of column support types

problems, including the largest problems, involving approximately 10,000 nodes, the *LimitState:SLAB* software was used; this software is freely available for academic use. To obtain rationalized solutions, the postprocessing step described by He and Gilbert (2016) was used, programmed in a *MATLAB* script. All results were obtained using an Intel i5-2310-based desktop PC with 6 GB RAM and running Microsoft *Windows 7*.

Numerical results are summarized in Table 1, which contains both DLO solutions obtained using dense nodal grids involving 10,000 nodes, to provide highly accurate solutions, and rationalized DLO solutions, which are easier to interpret visually. For problems with known analytical solutions, the margin of error was always found to be well within 1%. For other problems the results obtained in the present paper were found to be more accurate (i.e., lower) than those obtained using the numerical methods described in the existing literature. Additional details of each problem considered are provided in the following sections.

Singly Reinforced Slabs

Slabs that are singly reinforced (i.e., having no hogging resistance) will be considered first; these are of particular interest because the critical failure mechanism is likely to involve so-called corner levers or corner fans [which are often ignored by practicing engineers, who may instead pragmatically apply a margin of safety of, e.g., 10% (Kennedy and Goodchild 2004) to account for this and other simplifications].

Isotropic Six-Sided Slabs

The six-sided slabs shown in Figs. 8 and 9 were previously analyzed by Wüst and Wagner (2008). In both cases, $m_{px}^+ = m_{py}^+$ and $m_{px}^- = m_{py}^- = 0$ (i.e., there is no resistance to hogging moments). It is evident that the yield-line patterns identified by Wüst and Wagner (2008), shown in Figs. 8(b) and 9(b), involve yield-lines that intersect each of the corners and, hence, do not include corner levers or corner fans. In contrast, corner fans are evident in both the standard DLO solutions [Figs. 8(c) and 9(c)] and the rationalized DLO solutions [Figs. 8(d) and 9(d)]. Comparing the solutions obtained by Wüst and Wagner (2008) and those obtained using DLO, it is evident that the former are more than 10% higher than the latter (using 10,000 node DLO solutions provided here as

benchmarks, differences for the two problems are as follows: $(17.75/15.953 - 1) \times 100\% = 11.3\%$ and $(54.4/47.424 - 1) \times 100\% = 14.7\%$), indicating that using the yield-line patterns identified by Wüst and Wagner (2008) would be nonconservative, even if the usual 10% margin of safety were applied.

Orthotropic Trapezoidal Slab

The trapezoidal slab shown in Fig. 10 was previously analyzed by Balasubramanyam and Kalyanaraman (1988). The slab is orthotropically reinforced and simply supported on three sides. The relatively simple yield-line pattern identified by Balasubramanyam and Kalyanaraman (1988), shown in Fig. 10(b), does not include corner levers or corner fans and corresponds to a required moment capacity of $m_{px}^+ = 11.84q$. In contrast, the DLO solution shown in Fig. 10(c) is more complex and corresponds to a required moment capacity that is 18% higher [using the most accurate DLO solution available here, $(13.97/11.84 - 1) \times 100\% = 18\%$]. This again indicates that application of the usual 10% margin of safety would be insufficient to ensure a safe design.

Slabs with Internal Supports

Roof Slab

The slab shown in Fig. 11 has two external column supports and two knife-edge supports. The problem was originally analyzed by Bäcklund (1973), then by Munro and Da Fonseca (1978), and subsequently by Balasubramanyam and Kalyanaraman (1988). The rationalized DLO solution is shown in Fig. 11(c). A local failure can be observed near one external column; additionally, a fan-type mechanism is developed near the knife-edge supports. Though the slab is not anchored to the knife-edge supports, the failure mechanism shows no uplift of the slab.

Johansen's Slab with Point Supports

Johansen (1943) investigated a slab having two point supports [Fig. 12(a)]. Ideally a point support acts as a fulcrum, providing no rotational restriction and permitting uplift without necessitating plastic deformation of the slab. However, in DLO a point support is most conveniently modeled as a column of finite, though small, size [Fig. 12(b)]. This means that care must be exercised since, if a

Table 1. Summary of DLO versus Literature Solutions

Description	Literature		DLO				Deviation ^a (%)
	Source	Load factor	≤2,000 nodes (rationalized)	5,000 nodes	10,000 nodes		
Six-sided slab (Configuration 1)	Wüst and Wagner (2008)	17.750	15.970	15.956	15.953	11.27	
Six-sided slab (Configuration 2)	Wüst and Wagner (2008)	54.400	47.501	47.469	47.424	14.71	
Trapezoidal slab	Balasubramanyam and Kalyanaraman (1988)	0.084459 ^b	0.071928	0.071633	0.071566	18.02	
Roof slab	Backlund (1973)	0.38000	0.36028	0.35989	0.35863	5.96	
	Munro and Da Fonseca (1978)	0.40000				11.54	
	Balasubramanyam and Kalyanaraman (1988)	0.40200				12.09	
Johansen's slab with column support	Johansen (1943)	1.0411 ^b	1.0420 ^c	1.0420 ^c	1.0420 ^c	-0.08	
Point load near boundary (Configuration 1)	Johansen (1943)	11.425 ^d	11.443	11.442	11.435	-0.09	
Point load near boundary (Configuration 2)	Johansen (1943)	6.2832 ^d	6.3034	6.2990	6.2943	-0.18	
Slab with two-point loads (Configuration 1)	Johansen (1943)	11.420 ^d	11.458	11.452	11.448	-0.24	
Slab with two-point loads (Configuration 2)	Johansen (1943)	10.480 ^d	10.515	10.512	10.503	-0.22	
Slab loaded along a line (Configuration 1)	Johansen (1943)	19.200	18.867	18.861	18.847	1.87	
Slab loaded along a line (Configuration 2)	Johansen (1943)	12.700	11.693	11.672	11.646	9.05	
Cantilever slab loaded along a line (Configuration 1)	Johansen (1968)	10.460	9.816	9.804	9.795	6.79	
Cantilever slab loaded along a line (Configuration 2)	Johansen (1968)	6.3600	5.8393	5.8172	5.8086	9.49	
Ramsay's slab with patch load	Ramsay and Johnson (1998)	49.500	48.054	47.871	47.851	3.45	
Real-world slab ($i = 0$ for 215 mm blade columns)	Kennedy and Goodchild (2004)	0.020576 ^b	0.020246	0.020083	0.020020	2.78	
Real-world slab ($i = 0$ for 215 mm blade columns)	Kennedy and Goodchild (2004)	0.020576 ^b	0.019354	0.019138	0.019068	7.91	
Ramsay's L-shaped slab simply supported on three sides	Ramsay and Johnson (1998)	0.58824 ^b	0.42118	0.42125	0.42119	39.66	

Note: DLO = discontinuity layout optimization.

^aDifference between literature and DLO 10,000 node solution (using DLO solution as benchmark).

^bConverted to a load factor by multiplying by $1/m_p$.

^cInternal column support size $\mu = 0.001$ (Type II).

^dExact solution.

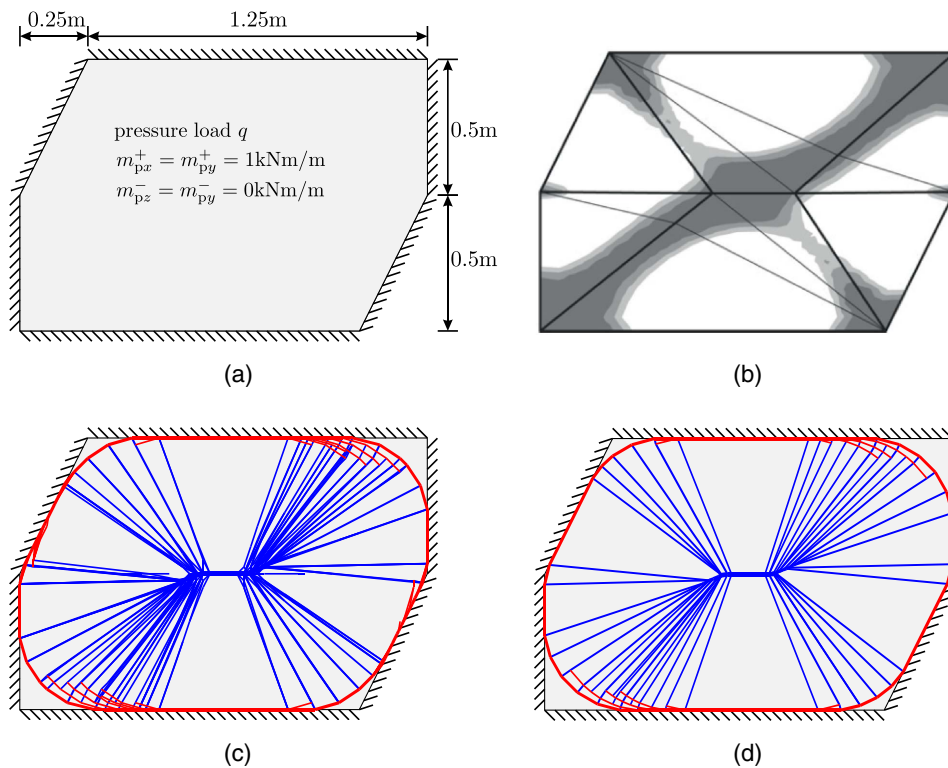


Fig. 8. Six-sided plate (Configuration 1): (a) problem specification; (b) yielding zone and yield-line pattern, $q = 17.75 \text{ kN/m}^2$ [reprinted from *Engineering Structures*, 30(7), Jochen Wüst and Werner Wagner, “Systematic prediction of yield-line configurations for arbitrary polygonal plates,” pp. 2081–2093, Copyright 2008, with permission from Elsevier]; (c) 2,000 node DLO yield-line pattern, $q = 15.992 \text{ kN/m}^2$ (when 10,000 nodes were used $q = 15.953 \text{ kN/m}^2$); (d) DLO yield-line pattern (rationalized, based on 2,000 node solution), $q = 15.970 \text{ kN/m}^2$

column restricts translational displacement of the slab along all its edges (e.g., a Type I or III column in Fig. 7), plastic deformation must occur near the column when uplift behavior occurs. In contrast, a Type II column behaves similarly to a point support, except that the fulcrum has been offset from the initial position [cf. Fig. 12(a)]. The influence of the support type and column size μ on the critical yield-line pattern is shown in Fig. 13. The following observations may be made:

- First, when a relatively small column size is used ($\mu = 0.001$), the resulting global yield-line pattern is largely insensitive to column type. However, local mechanisms are found close to Types I and III columns, and nonanchored (Type II) columns provide the best approximation of a point support;
- Second, when larger columns are used ($\mu = 0.2$), it is clear that the size of the column affects the failure mode significantly: a fan-type mechanism is developed near the Types I and III columns, and the uplift disappears. In contrast, uplift remains when Type II columns are involved, though the failure mechanism is different from that observed when a very small column size is present; and
- Third, when relatively large columns are used ($\mu = 0.5$), yield-lines develop along the column edges and no uplift is observed regardless of which of the three support types are used. In this case, the same failure mechanism is observed irrespective of whether Type I or II columns are present.

Slabs with Point and Line Loads

Several slab problems involving point loads considered by Johansen (1943) are now revisited using DLO. The resulting

yield-line patterns shown in Fig. 14 resemble closely the analytical solutions given by Johansen, with the margin of error being less than 1% (see also Table 1).

When line loads are present, fan-type mechanisms will often develop in the vicinity of the load. Examples originally considered by Johansen (1943, 1968) are analyzed here using DLO; the resulting yield-line patterns shown in Fig. 15 match Johansen’s results closely, though the DLO solutions are more accurate.

Slabs with Patch Loads

The slab problem shown in Fig. 16 is taken from Ramsay and Johnson (1998); this involves self-weight and a patch load Q . Using geometry optimization, Ramsay and Johnson (1998) obtained a relatively accurate solution of $Q = 49.5 \text{ kN}$ (which is only 3.5% higher than the 10,000 node DLO solution $Q = 47.85 \text{ kN}$). However, the process used by Ramsay and Johnson (1998) was cumbersome in that it involved identifying a suitable yield-line pattern for use in the geometry optimization stage. In contrast, the yield-line pattern shown in Fig. 16(c) was identified using DLO in a matter of seconds, without human intervention.

Real-World Slab

To further demonstrate the efficacy of DLO, the floor slab employed in a real-world building (Fig. 17) is now considered. The floor slab in question was also considered by Kennedy and Goodchild (2004), though for the purposes of this study full dimensions of the slab have been obtained from the original designers,

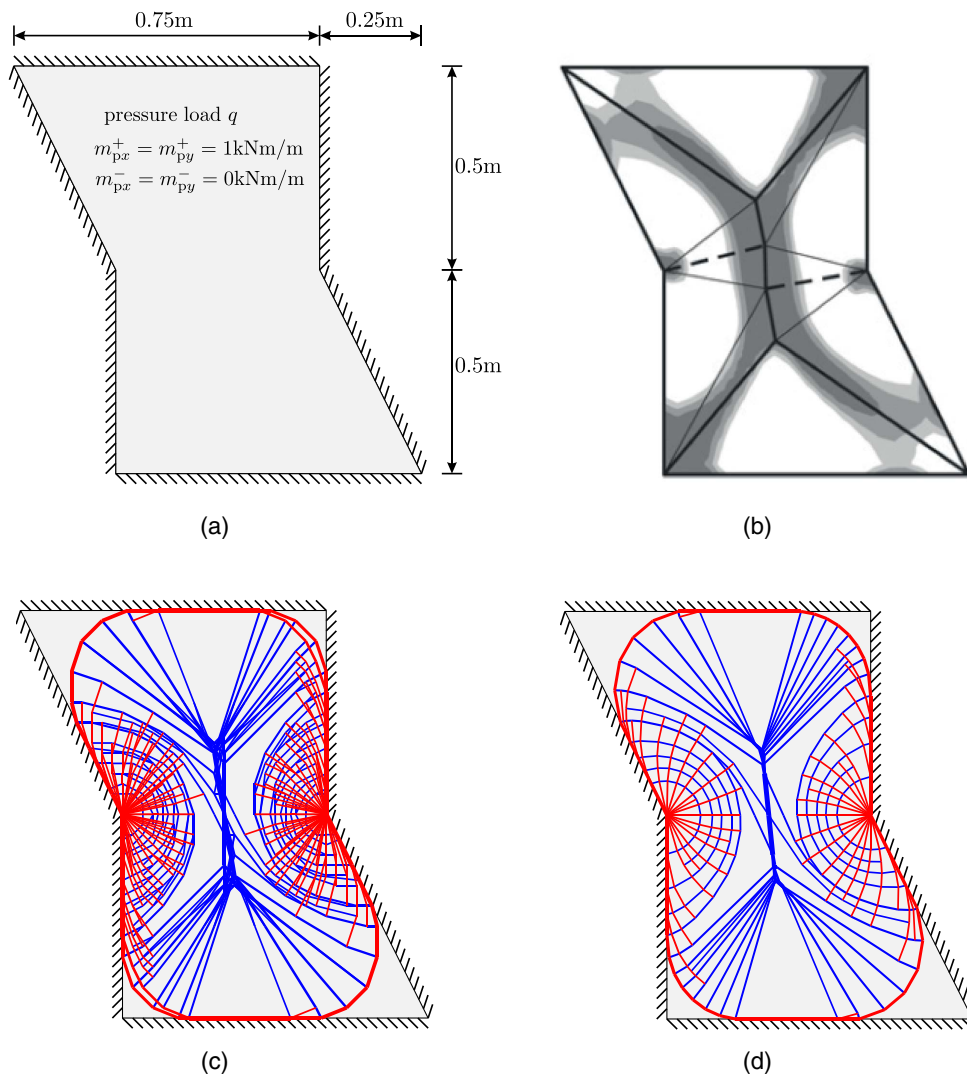


Fig. 9. Six-sided plate (Configuration 2): (a) problem specification; (b) yielding zone and yield-line pattern, $q = 54.4 \text{ kN/m}^2$ [reprinted from *Engineering Structures*, 30(7), Jochen Wüst and Werner Wagner, “Systematic prediction of yield-line configurations for arbitrary polygonal plates,” pp. 2081–2093, Copyright 2008, with permission from Elsevier]; (c) 2,000 node DLO yield-line pattern, $q = 47.745 \text{ kN/m}^2$ (when 10,000 nodes were used $q = 47.424 \text{ kN/m}^2$); (d) DLO yield-line pattern (rationalized, based on the 2,000 node solution), $q = 47.501 \text{ kN/m}^2$

Powell Tolner & Associates Ltd. This has allowed an accurate slab model to be created; full details are provided in Appendix II. A piecewise linear representation of the curved balconies is used and the walls and ‘blade’ columns are modeled using Type III internal columns. Following the lead of Kennedy and Goodchild (2004), here a support strength of $i = 1$ is used to represent the walls around the core, and $i = 0$ for the wall around the stairs. To model the 215 mm wide blade columns, two scenarios are considered: (1) $i = 1$; and (2) $i = 0$ for a more conservative design.

The rationalized yield-line patterns obtained using DLO are shown in Fig. 18. The first pattern matches very closely with the ‘folding plate’ mechanism assumed to be critical in Kennedy and Goodchild (2004). However, in the DLO solution fan-type mechanisms also develop around certain columns, leading to 2.8% increase in the required moment capacity [comparing $m_p = 48.6 \text{ kNm/m}$ from Kennedy and Goodchild (2004) to the 10,000 node DLO solution: $(49.9492/48.6 - 1) \times 100\% = 2.8\%$, assuming a uniform applied pressure load of 21.7 kN/m^2]. Although the hand calculation result described in Kennedy and Goodchild

(2004) appears remarkably accurate, it is worth noting that the process involved manually analysing 11 potential yield-line patterns, each postulated by an experienced engineer. In contrast when using DLO the yield-line patterns are identified automatically. Regarding the second, more conservative scenario, taking $i = 0$ around the blade columns, the resulting yield-line pattern is similar, though there is now a 7.9% increase in the required moment capacity [comparing the Kennedy and Goodchild (2004) solution to the 10,000 node DLO solution: $(52.4439/48.6 - 1) \times 100\% = 7.9\%$].

Discussion

Characteristic Features of Yield-Line Patterns

Currently, an engineer analysing a slab using the yield-line method can draw upon well-established rules when postulating the critical yield-line pattern. As presented by Jones and Wood (1967), the basic rules are

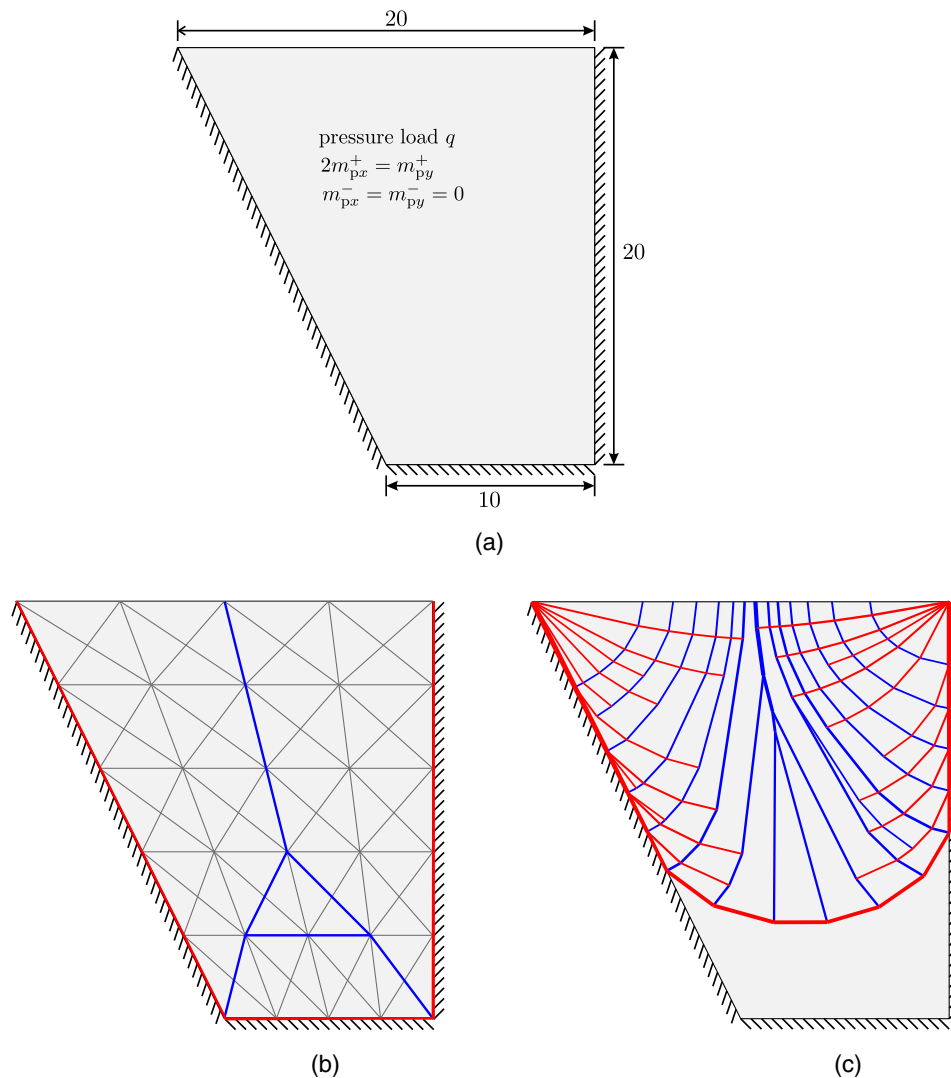


Fig. 10. Trapezoidal orthotropic slab: (a) problem specification; (b) yield-line pattern obtained by Balasubramanyam and Kalyanaraman (1988), $m_{px}^+ = 11.84q$; (c) DLO yield-line pattern (rationalized), $m_{px}^+ = 13.90q$ (10,000 node DLO solution, $m_{px}^+ = 13.97q$)

- Yield-lines are straight except where a region may become completely plastic at any point;
- The yield-line between two or more bordering rigid regions must pass through the intersection of the axes of rotation of these regions;
- Axes of rotation usually lie along supported edges or column lines; and
- Yield-lines may only change direction when intersecting another yield-line.

Gilbert et al. (2014), used observed features in DLO solutions, and then Mohr's circle analysis, to point out additional characteristic features of yield-line patterns for isotropically reinforced slabs:

- Yield-lines of opposite signs should intersect at 90° , whether in the interior of a slab or at a fixed support;
- Yield-lines of opposite signs should intersect simple supports and free edges at between 45° and 135° ; and
- Yield-lines of the same sign can intersect at any angle.

However, in the context of the present paper it is of interest to point out that the above relations can be generalized for orthotropically reinforced slabs by using the affine transformation method (Johansen 1943, 1968; Kennedy and Goodchild 2004; Nielsen and Hoang 2011); an example is shown in Fig. 19.

Problems Identifying Critical Yield-Line Patterns by Other Means

It is now clear that the DLO method provides a very efficient means of identifying critical yield-line patterns in the case of slabs with complex geometries, boundary conditions and/or load conditions. On the other hand it might be presumed that either hand-analysis or one of the previously proposed numerical procedures can be expected to provide reasonable solutions for simple slab analysis problems. However, as noted by Ramsay and Johnson (1997), this is not necessarily the case. Here two simple example problems encountered during the course of the present study will be used to investigate this issue.

Rectangular Slab Simply Supported on Two Adjacent Edges

When carrying out a yield-line analysis by hand, usually a yield-line pattern is postulated by hand [e.g., with the aid of the rules by Jones and Wood (1967)], and then the work method is used to obtain a solution. When using the work method various geometric parameters of a yield-line pattern can be adjusted to seek the minimum collapse load. For this reason, it might appear that the prescribed yield-line pattern need only be 'near correct'. Whilst in many cases use of a simple postulated yield-line pattern can lead

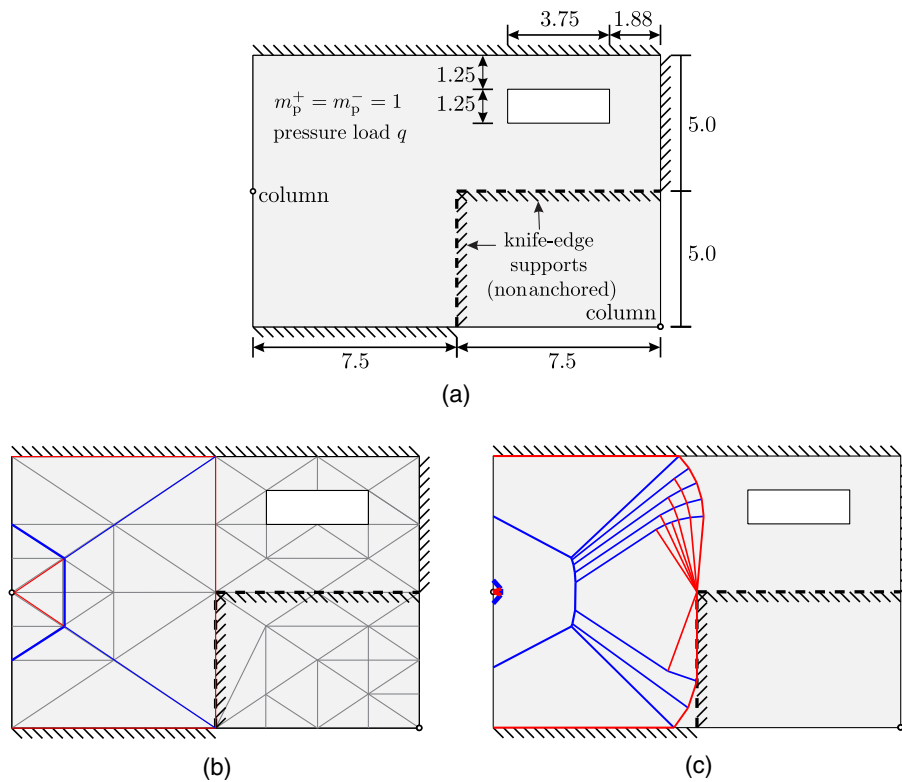


Fig. 11. Roof slab: (a) problem specification; (b) yield-line pattern, $\lambda = 0.4$ (adapted from Munro and Da Fonseca 1978); (c) DLO yield-line pattern (rationalized), $\lambda = 0.36028$ (10,000 node, DLO solution, $\lambda = 0.35863$)

to a reasonably accurate solution, an issue is that it can be very difficult to judge whether a prescribed yield-line pattern is truly 'near correct'.

For example, consider a seemingly simple example problem provided in Kennedy and Goodchild (2004), a rectangular slab which is simply supported on two adjacent edges [Fig. 20(a)]. Yield-line patterns provided in Johansen (1968) and Kennedy and Goodchild (2004) are shown in Figs. 20(b and c) respectively,

whilst the yield-line pattern identified using DLO is shown in Fig. 20(d). Note that in the case of the pattern shown in Fig. 20(c), geometric parameters of the pattern have been adjusted to find the minimum collapse load. The pattern shown in Fig. 20(b) leads to a relatively accurate solution, very similar to that derived using DLO, shown in Fig. 20(d). However, the solution shown in Fig. 20(c) is clearly very inaccurate; the reason for this will therefore now be investigated further.

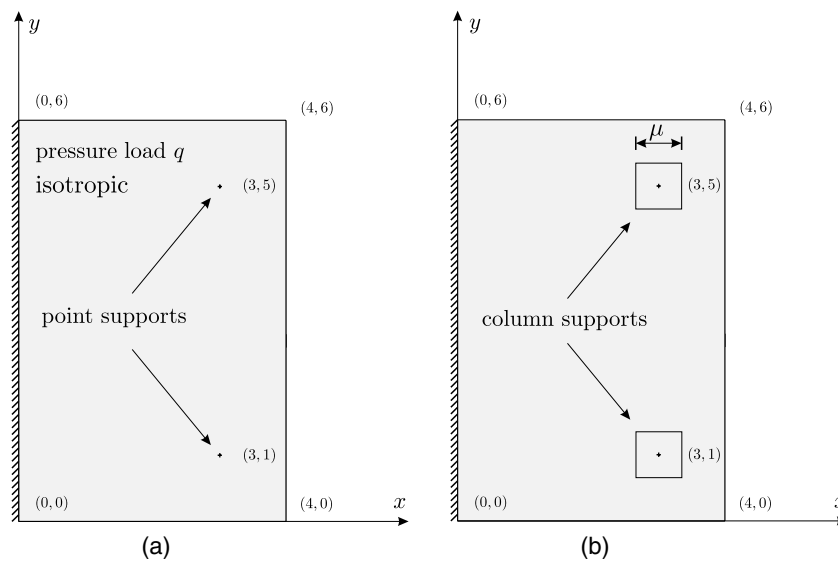


Fig. 12. Johansen's slab with columns (adapted from Johansen 1943): (a) original point supports in Johansen (1943); (b) square column supports from Fig. 7

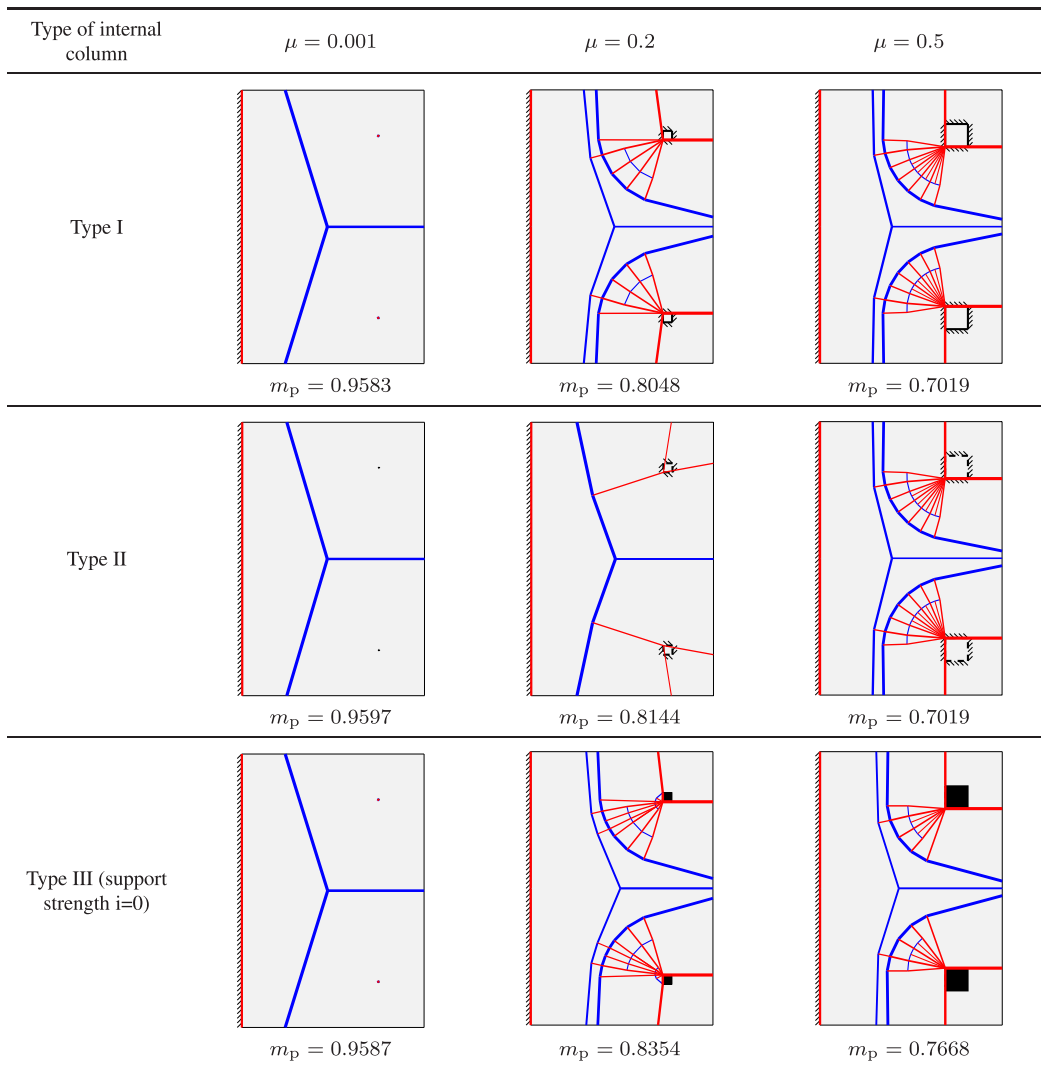


Fig. 13. Johansen's slab with column supports: rationalized DLO yield-line patterns obtained by varying support type and size

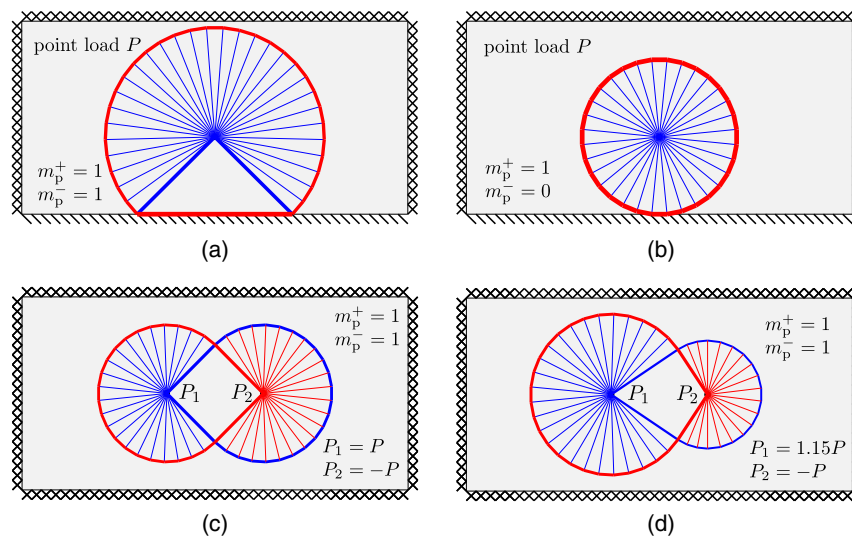


Fig. 14. Point loaded slabs—DLO yield-line patterns for (a) point load near boundary (Configuration 1), $P = 11.443$; (b) point load near boundary (Configuration 2), $P = 6.3034$; (c) slab with two point loads (Configuration 1), $P = 11.458$; (d) slab with two point loads (Configuration 2), $P = 10.515$ (see Table 1 for more accurate, 10,000 node, DLO solutions)

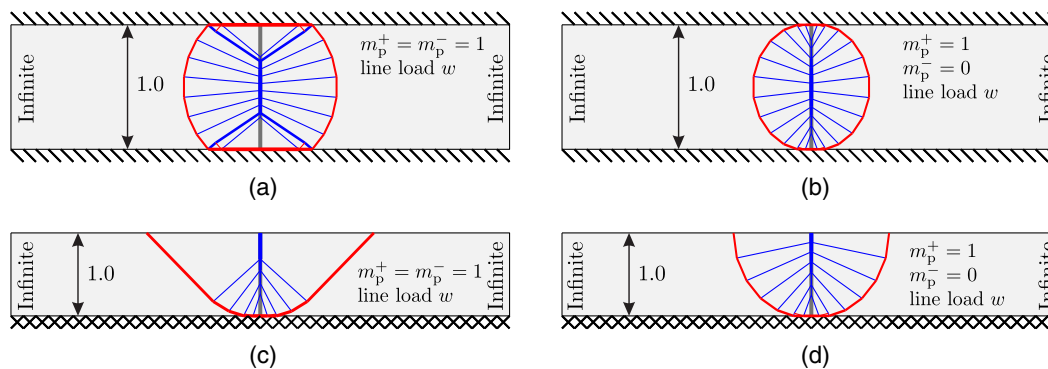


Fig. 15. Slabs loaded with line loads—DLO yield-line patterns for (a) slab loaded along a line (Configuration 1), $w = 18.867$; (b) slab loaded along a line (Configuration 2), $w = 11.693$; (c) cantilever slab loaded along a line (Configuration 1), $w = 9.816$; (d) cantilever slab loaded along a line (Configuration 2), $w = 5.8393$ (see Table 1 for more accurate, 10,000 node, DLO solutions)

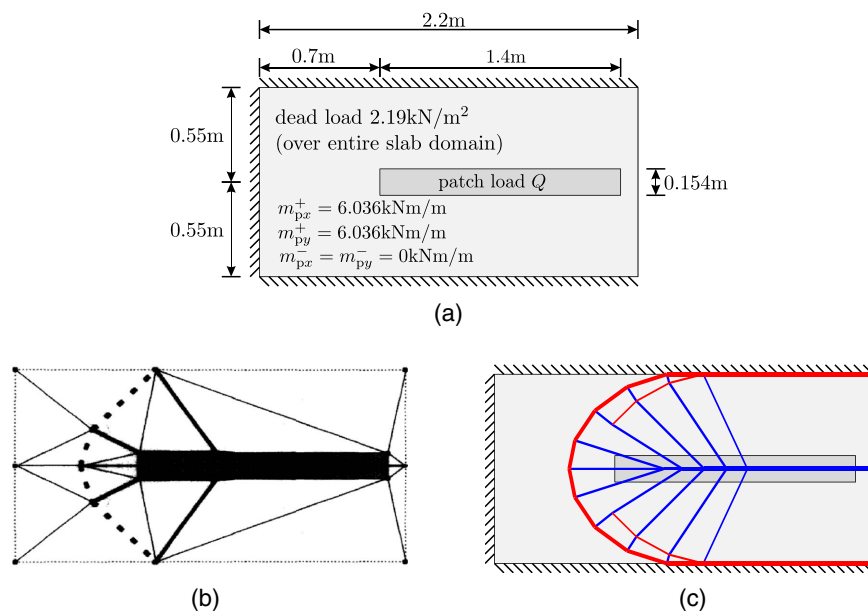


Fig. 16. Slab with central patch load [reprinted from *Engineering Structures*, 20(8), A.C.A. Ramsay and D. Johnson, “Analysis of practical slab configurations using automated yield-line analysis and geometric optimization of fracture patterns,” pp. 647–654, Copyright 1998, with permission from Elsevier]: (a) problem specification; (b) yield-line pattern obtained by Ramsay and Johnson (1998) using geometry optimization, $Q = 49.5$ kN; (c) DLO yield-line pattern (rationalized), $Q = 48.05$ kN (10,000 node DLO $Q = 47.85$ kN)

The geometry of the yield-line pattern given in Kennedy and Goodchild (2004) and shown in Fig. 20(c) is controlled by two geometric parameters ξ and η , as shown in Fig. 21(a). The required moment capacity m_p can be obtained by varying these parameters, as shown in Fig. 21(b). It can be noticed that for $0 < \xi \leq 9$, the maximum value of m_p is 168.0 kNm/m, which actually needs to be at least 52.9% higher for a safe design [calculated using $(256.9/168.0 - 1) \times 100\%$]. However, it is evident in Fig. 21 that from $\xi > 0$ to $\xi = 0$, the m_p values rise suddenly, showing the presence of a singularity. This implies that pattern in Fig. 20(c) does not transform smoothly to that shown in Fig. 20(b) simply by optimizing its geometric parameters (for example by using the ‘Solver’ optimization tool found in Microsoft *Excel*). This means that the yield-line pattern shown in Fig. 20(c) cannot really be considered to be “near correct”. This clearly demonstrates that large errors can easily be encountered

when using the yield-line method, even if the problem appears very simple. [Note that although the pattern shown in Fig. 20(c) was depicted in Kennedy and Goodchild (2004), the formula provided in that document actually corresponds to the pattern shown in Fig. 20(b)].

L-Shaped Slab

The L-shaped slab in figure Fig. 22(a) was investigated in Ramsay and Johnson (1998), using a rigid finite element based numerical analysis procedure. A relatively coarse mesh was used, leading to the yield-line pattern shown in Fig. 22(b) being identified. Although this pattern may appear qualitatively reasonable, the problem was recently revisited by Ramsay et al. (2015), who showed that the yield-line pattern is actually far from critical. The corresponding DLO yield-line pattern for this problem is shown in Fig. 22(c), which corresponds to a required m_p value of 2.3743 kNm/m. This is some 40% higher



Fig. 17. Real-world slab: used in a seven-story block of flats in London (image by authors)

than the solution given in the 1998 paper (1.70 kNm/m), showing that the latter solution was highly non-conservative. This indicates that, even for simple slab problems, the use of previously proposed numerical methods may lead to highly inaccurate solutions being obtained. It would also appear to show that it is difficult to qualitatively judge whether a given yield-line pattern is correct or otherwise (the highly inaccurate solution appears to have gone unnoticed in the literature for some 17 years, despite sustained interest in the field over that period). Fortunately the new DLO based automated yield-line analysis procedure overcomes accuracy issues associated with previously proposed numerical procedures (e.g., those utilizing rigid finite elements).

Conclusions

Discontinuity layout optimization (DLO) provides a powerful means of automating the yield-line method. Also, a given DLO solution, which can be complex in form, can be rationalized to aid

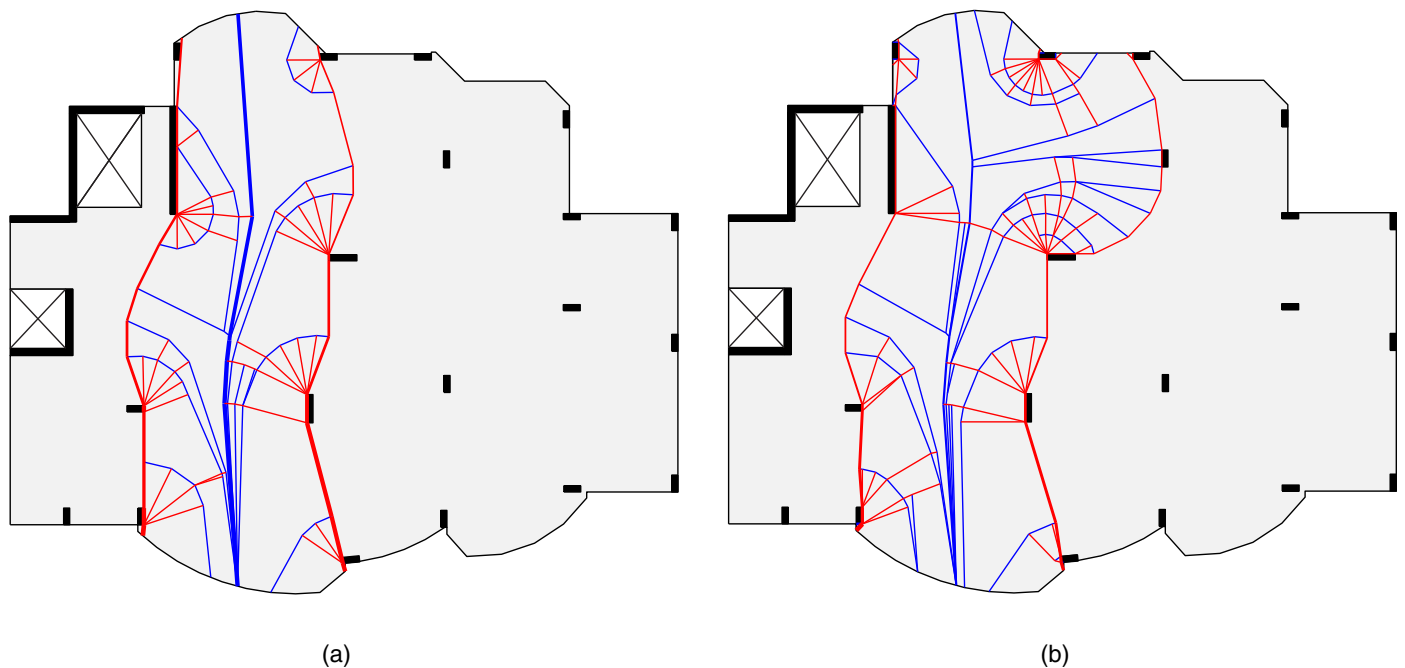


Fig. 18. Real-world slab: rationalized yield-line patterns using DLO, (a) $i = 1$ for 215 mm blade columns: $m_p = 49.3923$ kNm/m (10,000 node, DLO $m_p = 49.9492$ kNm/m); (b) $i = 0$ for 215 mm blade columns: $m_p = 51.6699$ kNm/m (10,000 node, DLO $m_p = 52.4439$ kNm/m)

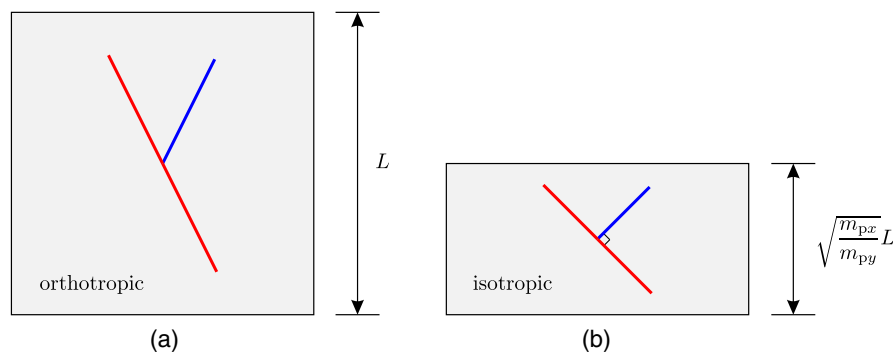


Fig. 19. Determining characteristic features of a yield-line pattern in an orthotropic slab: (a) original orthotropic slab; (b) equivalent isotropic slab derived using an affine transformation; the critical yield-line pattern in (b) will involve yield-lines of opposite sign intersecting at 90° ; the geometry of the yield-line pattern in (a) can be derived from (b) via geometrical transformation

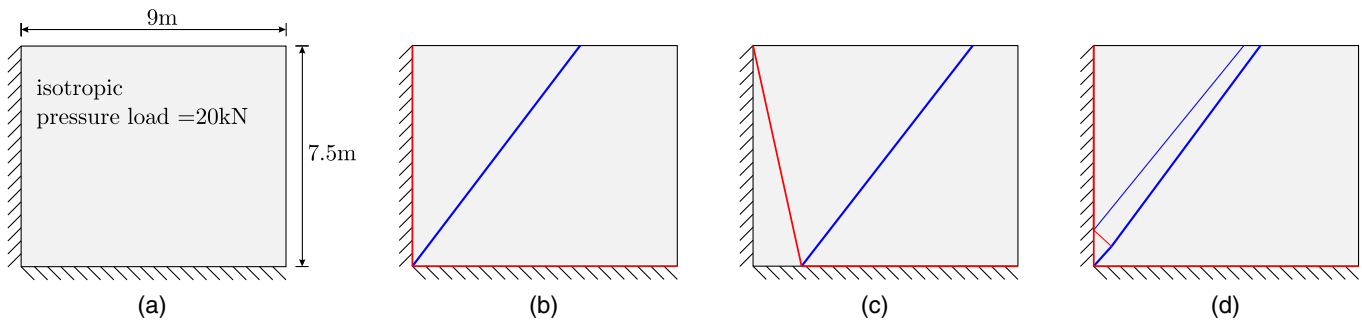


Fig. 20. Rectangular slab simply supported on two adjacent edges: (a) problem specification; (b) simple yield-line pattern, $m_p = 256.5$ kNm/m; (c) alternative yield-line pattern, obtained by “optimization,” $m_p = 168.0$ kNm/m; (d) DLO yield-line pattern (rationalized), $m_p = 256.9$ kNm/m

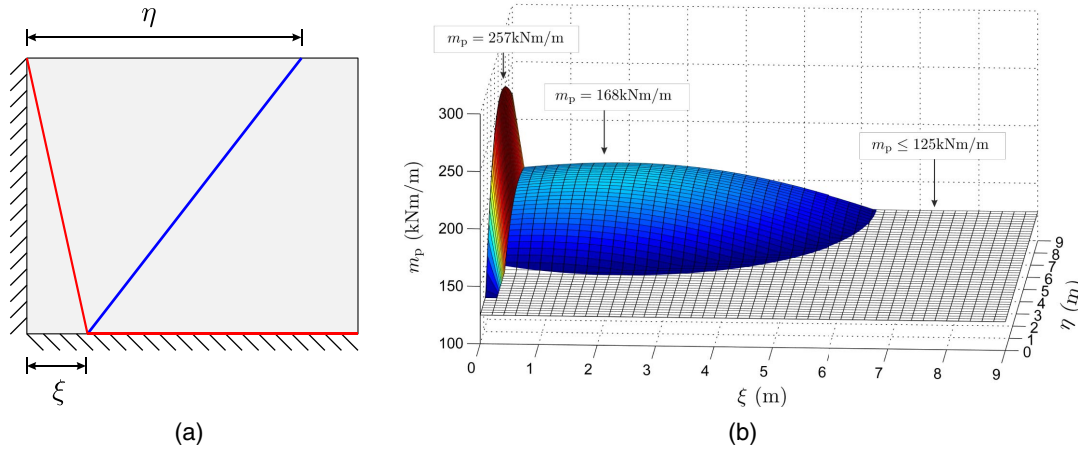


Fig. 21. Rectangular slab simply supported on two edges: parametric study for yield-line pattern proposed by Kennedy and Goodchild (2004): (a) relevant geometric parameters ξ , η ; (b) calculated required value of m_p by varying ξ and η

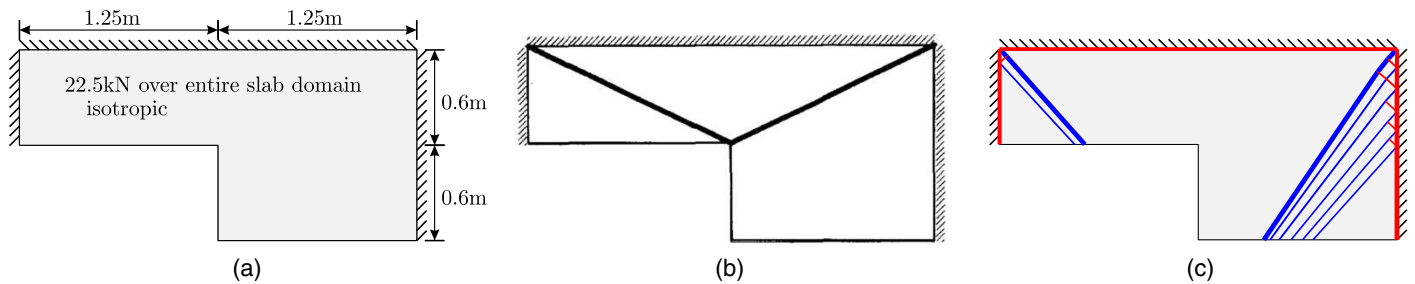


Fig. 22. Ramsay’s L-shaped slab simply supported on three sides: (a) problem specification; (b) yield-line pattern obtained by Ramsay and Johnson (1998), $m_p = 1.70$ kNm/m [reprinted from *Engineering Structures*, 20(8), A.C.A. Ramsay and D. Johnson, “Analysis of practical slab configurations using automated yield-line analysis and geometric optimization of fracture patterns,” pp. 647–654, Copyright 1998, with permission from Elsevier]; (c) DLO yield-line pattern (rationalized), $m_p = 2.3743$ kNm/m

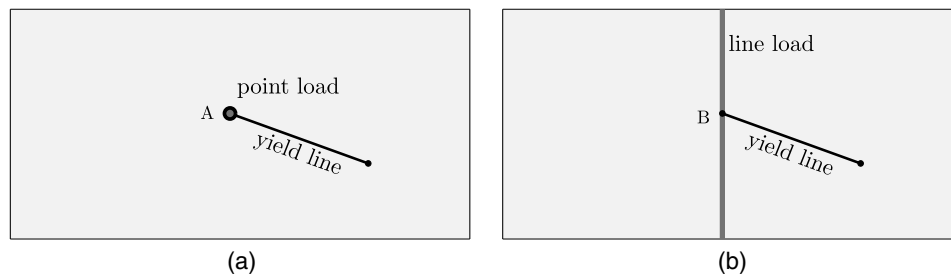


Fig. 23. Extra move limits imposed on nodes due to presence of point and line loads: (a) Node A is nonmovable because it coincides with a point load; (b) Node B can only move in the direction of the line load

visual interpretation and improve accuracy if required. In the present paper, it has been demonstrated that DLO can be applied to a wide variety of problems incorporating practical features (e.g., orthotropic reinforcement and a wide variety of support conditions and loading types). For all the example problems considered in the paper, DLO solutions have been found which are more accurate than those obtained using previously proposed upper bound numerical analysis techniques; in some cases this has shown that literature solutions are highly nonconservative.

Appendix I. Extra Considerations in Geometry Optimization

In geometry optimization, nodal positions (\mathbf{x} and \mathbf{y}) are considered as optimization variables, in addition to \mathbf{d} and \mathbf{p} in optimization problem (1). Therefore, the coefficient matrices and vectors in (1) contain the optimization variables, which are continuously updated during the optimization process. For example, whilst \mathbf{g} comprises constants coefficient values when slabs are isotropically reinforced, when orthotropic reinforcement is present the coefficient values are affected by the yield-line angles ϕ [see also Fig. 5 and yield-criterion (3)] that are determined by \mathbf{x} and \mathbf{y} ; hence \mathbf{g} is now a function of the optimization variables.

In addition, functions representing the load effect terms \mathbf{f}_L and \mathbf{f}_D can become nonsmooth with respect to nodal positions, which can cause problems. In this paper extra constraints are added to prevent these functions from becoming nonsmooth. Thus in Fig. 23(a) node A is made nonmovable since it coincides with a point load; in Fig. 23(b), node B is restrained so as to only be able to move in the direction of the line load. For patch loads, domain decomposition (which divides a slab domain into several separate sub-domains; see He and Gilbert 2016 for details) can be used, and a subdomain can be created in the patch load area. Note that the above approaches restrict nodal movements and will therefore potentially somewhat reduce the accuracy of the numerical solutions obtainable using geometry optimization.

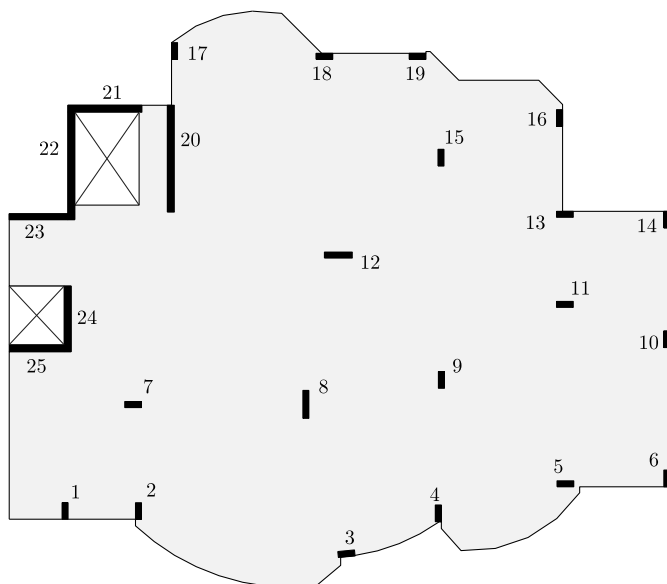


Fig. 24. Real-world slab: geometry and column ID

Appendix II. Geometric Data of the Real-World Slab

Vertices of the floor slab (Fig. 24) are given in Table 2. Dimensions of the holes are given in Table 3 and those of the blade columns in Table 4.

Table 2. Real-World Slab: Vertices of Polygonal Slab Domain (Units in Meters)

Identifier	x	y
1	-0.727	0.000
2	3.794	0.000
3	3.794	-0.238
4	4.466	-0.802
5	5.194	-1.291
6	5.971	-1.700
7	6.786	-2.022
8	7.632	-2.256
9	8.503	-2.398
10	9.384	-2.446
11	10.250	-2.400
12	11.143	-1.650
13	11.143	-1.427
14	11.143	-1.359
15	11.657	-1.296
16	12.460	-1.132
17	13.238	-0.874
18	13.980	-0.525
19	14.675	-0.090
20	14.748	-0.090
21	14.748	-0.335
22	15.456	-1.123
23	16.686	-1.046
24	17.855	-0.655
25	18.883	0.025
26	19.702	0.946
27	19.702	1.161
28	22.934	1.161
29	22.934	11.027
30	19.090	11.027
31	19.090	14.855
32	18.237	15.723
33	15.376	15.723
34	14.348	16.751
35	14.198	16.751
36	14.198	16.686
37	10.463	16.686
38	9.029	18.118
39	7.979	18.199
40	6.937	18.044
41	5.956	17.661
42	5.085	17.069
43	5.085	14.826
44	1.373	14.826
45	1.373	10.941
46	-0.727	10.941
47	-0.727	8.350
48	1.488	8.350
49	1.488	6.000
50	-0.727	6.000

Table 3. Real-World Slab: Locations of Holes (Units in Meters)

Description	x_1	y_1	x_2	y_2	x_3	y_3	x_4	y_4
Stair	1.623	11.250	3.925	11.250	3.925	14.576	1.623	14.576
Core	-0.727	6.250	1.238	6.250	1.238	8.350	-0.727	8.350

Table 4. Real-World Slab: Column Support Details (Units in Meters)

Column identifier	Scenario 1	Scenario 2	x_1	y_1	x_2	y_2	x_3	y_3	x_4	y_4
	support strength i	support strength i								
1	1	0	1.165	0.000	1.380	0.000	1.380	0.592	1.165	0.592
2	1	0	3.794	0.592	3.794	-0.008	4.009	-0.008	4.009	0.592
3	1	0	11.040	-1.157	11.060	-1.367	11.658	-1.316	11.638	-1.099
4	1	0	14.533	-0.090	14.748	-0.090	14.748	0.510	14.533	0.510
5	1	0	18.891	1.161	19.491	1.161	19.491	1.376	18.891	1.376
6	1	0	22.934	1.761	22.719	1.761	22.719	1.161	22.934	1.161
7	1	0	3.410	4.000	4.010	4.000	4.010	4.215	3.410	4.215
8	1	0	9.788	3.613	10.003	3.613	10.003	4.613	9.788	4.613
9	1	0	14.644	4.690	14.859	4.690	14.859	5.290	14.644	5.290
10	1	0	22.719	6.148	22.934	6.148	22.934	6.748	22.719	6.748
11	1	0	18.875	7.586	19.475	7.586	19.475	7.801	18.875	7.801
12	1	0	10.560	9.354	11.560	9.354	11.560	9.569	10.560	9.569
13	1	0	18.875	10.812	19.475	10.812	19.475	11.027	18.875	11.027
14	1	0	22.719	10.427	22.934	10.427	22.934	11.027	22.719	11.027
15	1	0	14.627	12.650	14.842	12.650	14.842	13.250	14.627	13.250
16	1	0	18.875	14.069	19.090	14.069	19.090	14.669	18.875	14.669
17	1	0	5.085	16.469	5.300	16.469	5.300	17.069	5.085	17.069
18	1	0	10.260	16.471	10.860	16.471	10.860	16.686	10.260	16.686
19	1	0	13.598	16.471	14.198	16.471	14.198	16.686	13.598	16.686
20	0	0	4.935	11.000	5.185	11.000	5.185	14.826	4.935	14.826
21	0	0	1.373	14.576	4.025	14.576	4.025	14.826	1.373	14.826
22	0	0	1.623	10.726	1.623	14.576	1.373	14.576	1.373	10.726
23	0	0	1.373	10.941	-0.727	10.941	-0.727	10.726	1.373	10.726
24	1	1	1.238	6.000	1.488	6.000	1.488	8.350	1.238	8.350
25	1	1	1.238	6.250	-0.727	6.250	-0.727	6.000	1.238	6.000

Acknowledgments

Initial work in the area of this study was undertaken while the second author was in receipt of an EPSRC Advanced Research Fellowship, Grant No. GR/S53329/01. The authors wish to thank Charles H. Goodchild from the U.K. Concrete Centre and John Sestak from Powell Tolner & Associates for providing the geometric data required for the analysis of the slab shown in Fig. 18.

Supplemental Data

Fig. S1, Table S1, *MATLAB* scripts, and an explanatory document are available online in the ASCE Library (www.ascelibrary.org).

References

- Anderheggen, E., and Knöpfel, H. (1972). "Finite element limit analysis using linear programming." *Int. J. Solids Struct.*, 8(12), 1413–1431.
- Bäcklund, J. (1973). "Finite element analysis of nonlinear structures." Ph.D. thesis, Chalmers Tekniska Högskola, Gothenburg, Sweden.
- Balasubramanyam, K. V., and Kalyanaraman, V. (1988). "Yield-line analysis by linear programming." *J. Struct. Eng.*, 10.1061/(ASCE)0733-9445(1988)114:6(1431), 1431–1437.
- Bleyer, J., and De Buhan, P. (2013). "On the performance of non-conforming finite elements for the upper bound limit analysis of plates." *Int. J. Numer. Meth. Eng.*, 94(3), 308–330.
- Chan, H. S. Y. (1972). "Collapse load of reinforced concrete plates." *Int. J. Numer. Meth. Eng.*, 5(1), 57–64.
- Gilbert, M., He, L., and Pritchard, T. (2015). "Yield-line method for concrete slabs: Automated at last." *Struct. Eng.*, 93(10), 44–48.
- Gilbert, M., He, L., Smith, C. C., and Le, C. V. (2014). "Automatic yield-line analysis of slabs using discontinuity layout optimization." *Proc. R. Soc. A*, 470(2168), 20140071.

- He, L., and Gilbert, M. (2016). "Automatic rationalization of yield-line patterns identified using discontinuity layout optimization." *Int. J. Solids Struct.*, 84(1), 27–39.
- Jackson, A. M., and Middleton, C. R. (2013). "Closely correlating lower and upper bound plastic analysis of real slabs." *Struct. Eng.*, 91(1), 34–40.
- Johansen, K. W. (1943). *Brudlinieteorier (yield-line theory)*, Cement and Concrete Association, London.
- Johansen, K. W. (1968). *Pladeformler (yield-line formulae for slabs)*, Cement and Concrete Association, London.
- Johnson, D. (1994). "Mechanism determination by automated yield-line analysis." *Struct. Eng.*, 72(19), 323–327.
- Johnson, D. (1995). "Yield-line analysis by sequential linear programming." *Int. J. Solids Struct.*, 32(10), 1395–1404.
- Jones, L. L., and Wood, R. H. (1967). *Yield-line analysis of slabs*, American Elsevier Publishing, New York.
- Kennedy, G., and Goodchild, C. H. (2004). *Practical yield-line design*, Concrete Centre, Surrey, U.K.
- Krabbenhoft, K., and Damkilde, L. (2003). "A general non-linear optimization algorithm for lower bound limit analysis." *Int. J. Numer. Meth. Eng.*, 56(2), 165–184.
- Le, C. V., Gilbert, M., and Askes, H. (2010). "Limit analysis of plates and slabs using a meshless equilibrium formulation." *Int. J. Numer. Meth. Eng.*, 83(13), 1739–1758.
- LimitState:SLAB [Computer Software]. LimitState Ltd., Sheffield, U.K.
- MATLAB* [Computer software]. MathWorks, Natick, MA.
- Maunder, E. A. W., and Ramsay, A. C. A. (2012). "Equilibrium models for lower bound limit analyses of reinforced concrete slabs." *Comput. Struct.*, 108–109, 100–109.
- Middleton, C. R. (1997). "Concrete bridge assessment: An alternative approach." *Struct. Eng.*, 75(23/24), 403–409.
- Munro, J., and Da Fonseca, A. M. A. (1978). "Yield-line method by finite elements and linear programming." *Struct. Eng.*, 56(2), 37–44.
- Nielsen, M. P., and Hoang, L. C. (2011). *Limit analysis and concrete plasticity*, 3rd Ed., Taylor & Francis Group, Boca Raton, FL.

- Ramsay, A., Maunder, E., and Gilbert, M. (2015). *Yield-line analysis of reinforced concrete slabs: Is the 10% rule safe?* National Agency for Finite Element Methods and Standards Benchmark Magazine, Hamilton, Lanarkshire, Scotland, 15–20.
- Ramsay, A. C. A., and Johnson, D. (1997). “Geometric optimization of yield-line patterns using a direct search method.” *Struct. Optim.*, 14(2), 108–115.
- Ramsay, A. C. A., and Johnson, D. (1998). “Analysis of practical slab configurations using automated yield-line analysis and geometric optimization of fracture patterns.” *Eng. Struct.*, 20(8), 647–654.
- Smith, C., and Gilbert, M. (2007). “Application of discontinuity layout optimization to plane plasticity problems.” *Proc. R. Soc. A*, 463(2086), 2461–2484.
- Thavalingam, A., Jennings, A., Sloan, D., and McKeown, J. J. (1999). “Computer-assisted generation of yield-line patterns for uniformly loaded isotropic slabs using an optimisation strategy.” *Eng. Struct.*, 21(6), 488–496.
- Wüst, J., and Wagner, W. (2008). “Systematic prediction of yield-line configurations for arbitrary polygonal plates.” *Eng. Struct.*, 30(7), 2081–2093.